Structural Engineering and Mechanics, *Vol. 75, No. 1 (2020) 71-86*
DOI: https://doi.org/10.12989/sem.2020.75.1.071

Experimental and numerical studies on mechanical behavior of buried pipelines crossing faults

Dan F. Zhang[1,2a], Xue M. Bie[1,3b], Xi. Zeng[1,2c], Zhen. Lei[1,2d] and Guo F. Du*[1,2]

[1]*School of Urban Construction, Yangtze University, Jingzhou 434000, China*
[2]*Hubei Provincial Oil and Gas Storage and Transportation Engineering Technology Research Center, Jingzhou 434000, China*
[3]*State Key Laboratory of Coastal and Offshore Engineering, Dalian University of Technology, Dalian 116024, China*

(Received October 19, 2019, Revised January 10, 2020, Accepted January 11, 2020)

Abstract. This paper presents a study on the mechanical behavior of buried pipelines crossing faults using experimental and numerical methods. A self-made soil-box was used to simulate normal fault, strike-slip fault and oblique slip fault. The effects of some important parameters, including the displacement and type of fault, the buried depth and the diameter of pipe, on the deformation modes and axial strain distribution of the buried pipelines crossing faults was studied in the experiment. Furthermore, a finite element analysis (FEA) model of spring boundary was developed to investigate the performance of the buried pipelines crossing faults, and FEA results were compared with experimental results. It is found that the axial strain distribution of those buried pipelines crossing the normal fault and the oblique fault is asymmetrical along the fault plane and that of buried pipelines crossing the strike-slip fault is approximately symmetrical. Additionally, the axial peak strain appears near both sides of the fault and increases with increasing fault displacement. Moreover, the axial strain of the pipeline decreases with decreasing buried depth or increasing ratios of pipe diameter to pipe wall thickness. Compared with the normal fault and the strike-slip fault, the oblique fault is the most harmful to pipelines. Based on the accuracy of the model, the regression equations of the axial distance from the peak axial strain position of the pipeline to the fault under the effects of buried depth, pipe diameter, wall thickness and fault displacement were given.

Keywords: crossing fault; buried pipeline; strain distribution; deformation mode; finite element analysis (FEA); position of peak axial strain

1. Introduction

As an efficient means to transport gaseous and liquid materials, pipelines are widely deployed and play important roles in a nation's economy. However, the safety operation of a pipeline is challenged by many adverse effects (Kishawy and Gabbar 2010), such as corrosion (Du *et al*. 2016a, Liu *et al*. 2019), erosion (Wang *et al*. 2019), cracks (Du *et al*. 2013), and external impacts (Jiang *et al*. 2019, Dong *et al*. 2019). For buried pipelines, fault movement threatens the pipeline integrity and easily causes large deformation and damages to pipelines (Vazouras *et al*. 2012, Cheng *et al*. 2019, Wu *et al*. 2019). Benefitting from the recent rapid development of structural health monitoring technology (Yi *et al*. 2015, Zeng *et al*. 2015, Lynch *et al*. 2004, Zhang *et al*. 2018, Zhang *et al*. 2018), pipeline monitoring receives much attention (Ho *et al*. 2019, Ren *et al*. 2018, Arzaghi *et al*. 2017, Jia *et al*. 2018a, Zhu *et al*. 2017). The advanced sensing technologies, such as fiber optic sensors (Jia *et al*. 2018b, Hou *et al*. 2014, Ren *et al*. 2014, Jia *et al*. 2015) and piezoceramic transducers (Du *et al*. 2016b, Xu *et al*. 2019, Du *et al*.2017), also contribute to the pipeline monitoring. In addition, finite element analysis (FEA) and experimental studies have been carried out to study the performance of the pipeline (Zhang *et al*. 2016, Jalali t al. 2016, Xu and Lin 2017).

With the increasing emphasis of the lifeline earthquake engineering, which mainly includes water supply and drainage, oil and gas transportation and other energy supply systems engineering (Ha *et al*. 2010, Zhang *et al*. 2017, Arafah *et al*. 2015), research have been conducted to study the force mechanism of the pipeline under fault movement. Newmark and Hall (1975) developed the Newmark-Hall method for calculating buried pipelines crossing fault. This method neglects bending deformation of pipelines and transverse pipeline-soil interactionl, resulting in the obtained pipeline strain being smaller than the actual one. Subsequently, Kennedy *et al*. (1997) further improved this method by considering both bending deformation of pipeline and transverse pipeline-soil interaction. With the development of finite element technology, many scholars have applied finite element analysis method to this field. ASCE: Guideline for the seismic design of oil and gas pipeline systems (1984) recommended adopting finite

*Corresponding author, Professor
E-mail: gfdu@yangtzeu.edu.cn
a M.Sc Student
E-mail: 201872379@yangtzeu.edu.cn
b Ph.D
E-mail: xmb@mail.dlut.edu.cn
c M.Sc Student
E-mail: 201672335@yangtzeu.edu.cn
d M.Sc Student
E-mail: 201672325@yangtzeu.edu.cn.

ISSN: 1225-4568 (Print), 1598-6217 (Online)

element method to analyze the strain response of buried pipelines crossing fault. Then, Wang and Yeh (1985) improved the Kennedy's method by adopting elastic foundation beam to simulate large deformation section of pipeline. Subsequently, Takada *et al*. (2001) analyzed the relationship between strain and bending angle of buried pipeline under normal fault and reverse fault by using shell-beam hybrid model and proposed the calculation method of peak strain of pipeline under different fault crossing angle. For further research, Cocchetti *et al*. (2008) explored the relationship among pipe size, crossing angle and displacement on the basis of the pipe shell model. Liu *et al*. (2009) used shell element and solid element to simulate pipe-soil model and analyze the buckling response and variation trend of pipelines under the influence of diameter and crossing angle. Vazouras *et al*. (2015) considered the length and crossing angle of the pipeline when building the numerical model. Using the proposed closed-form nonlinear force-displacement relationship compared the axial strains with those obtained from detailed finite element models. It is shown that the end conditions of the pipeline have a significant influence on pipeline performance. In addition, Halabian and Tohid (2018) used large deformation shell elements to simulate the pipeline embedded in the near field soil and used elastic beam elements to simulate the segment located far away from the fault. Developing a new hybrid model and applied it to solve rigorous soil-pipeline interaction. At the same time, many scholars have studied the cross-fault pipeline through experiments. Audibert and Nyman (1977) used hydraulic device to push the self-made pipe soil device to simulate fault movement, then, the analysis method of load-displacement curve of buried pipeline was proposed under the influence of different parameters. Subsequently, Erami *et al*. (2015) adopted full-scale experiments to research the applicability of pipe-soil interaction equations to pipelines. The results of full-scale experiments were compared to the results of computer-aided analyses. It shows that the nature of soil in the pipe-soil interaction and the effects of connection joints must be considered. In addition, Rofooei *et al*. (2015) analyzed the deformation and buckling behavior of steel pipes and HDPE pipes by simulating reverse faults with full-scale experiment device and the influence of fault and pipeline parameters on pipeline strain was discussed in detail. Recently, Zeng *et al*. (2019) used self-made scale model and equivalent spring to analyze the influence of soil type on the mechanical behavior of the pipeline under fault movement. The results show that choice the non-adhesive backfill can decrease the strain and deformation of the pipeline.

The above research results show that fault movement has great influence on the mechanical behavior of buried pipelines crossing faults. However, in the scale model test, the axial tension of area far away from the fault on the pipeline was not considered, furthermore, few people study it by experimental methods and the research parameters are relatively less. Therefore, a systemic investigation into the mechanical behavior of buried pipelines crossing faults is presented in the paper, incorporating experimental study and FE modeling. An experimental study on nine buried steel pipelines crossing fault was conducted by using a soil-box scale test device with spring boundary that considers the small axial deformation occurred at the area far away from the fault on the pipelines. The effects of some important parameters on the deformation modes and axial strain distribution of the buried pipelines crossing fault were obtained. Finally, a finite element analysis (FEA) model on soil-pipeline was developed for further research the properties of buried pipeline crossing fault and its accuracy was verified by experimental results. Based on the accuracy of the model, the variation law of the axial distance from the peak axial strain position of the pipeline to the fault under the effects of buried depth, pipe diameter, wall thickness and fault displacement was studied, and the regression equations of the axial distance from the peak axial strain position of the pipeline to the fault were given.

2. Experimental program

2.1 Experimental design

Two kinds of pipes with the diameter of 32mm and 40mm were used in the test, of which both the thicknesses were 2.3mm. Referring to the model similarity design in the reference (Zeng *et al*. 2019), the longitudinal length of pipeline should be no less than $L = 60D \approx 60 \times 0.040 = 2.4m$, and the minimum width of the soil-box should be $b = 3/(58/15) = 0.78m$. Thus, the total length of the pipeline and soil-box utilized in this test was defined as 3.0 m, the width of the soil-box was defined as 1.0 m, and the height of the soil-box was defined as 1.1m considering the effect on the pipeline's mechanical properties for various buried depth. Therefore, the dimension of soil-box is 3.0 m (length) × 1.0 m (width) × 1.1 m (height), with a buried depth defined as 0.3m and 0.6m for the pipeline. Nine buried pipeline specimens were designed and fabricated for the test. Table 1 presents the cross-sectional dimensions and the fault parameters of all specimens. As shown in Table 1, all specimens are labeled to identify the diameter, buried depth and fault type. For example, the label "N-32-0.3" is defined as follows:

The first part "N" represents that the fault type of specimen is normal fault.

The second part "32" indicates the pipeline with diameter (D) of 32 mm.

The last part "0.3" means that the buried depth (d) of specimens is 0.3 m.

When laying soil, the clay was filled in the soil-box with a thickness of 5cm each time, followed by levelling and compacting with certain devices before the succeeding procedure of another layer. The laid soil was then left still for 48 hours after the entire process of laying soil was completed, and check whether the strain gauges in good work condition during the period. To accurately study the mechanical behavior of buried pipelines crossing fault, both the axial tension on the pipeline of large deformation section near fault and small deformation section far away from fault should be fully considered. Therefore, in this experiment, the screw and spring were arranged at the ends

Table 1 Details of specimens

No.	Specimen	Fault type	*D*/mm	*t*/mm	*L*/mm	Crossing angle / (°)	Spring elastic coefficient / (N/m)	*d*/m
1	N-32-0.3	Normal fault	32	2.3	3000	90	4729	0.3
2	N-32-0.6	Normal fault	32	2.3	3000	90	4729	0.6
3	N-40-0.3	Normal fault	40	2.3	3000	90	4729	0.3
4	S-32-0.3	Strike-slip fault	32	2.3	3000	90	4729	0.3
5	S-32-0.6	Strike-slip fault	32	2.3	3000	90	4729	0.6
6	S-40-0.3	Strike-slip fault	40	2.3	3000	90	4729	0.3
7	O-32-0.3	Oblique slip fault	32	2.3	3000	90	4729	0.3
8	O-32-0.6	Oblique slip fault	32	2.3	3000	90	4729	0.6
9	O-40-0.3	Oblique slip fault	40	2.3	3000	90	4729	0.3

*Notes: *D*, *t*, *L* and *d* denotes diameter, wall thickness, length and buried depth of the pipeline respectively.

Fig. 1 Design at the pipeline end

Fig. 2 Spring device

Table 2 Material properties of soil

Soil type	Natural density (g/cm3)	Water content (%)	Internal friction angle (°)	cohesion (kpa)	Poisson ratio
Clay	1.88	26.8	7.8	35.5	0.35

Table 3 Mechanical properties of pipelines

Pipeline diameter /mm	Wall thickness /mm	Yield strength /MPa	Tensile strength /MPa	Modulus of elasticity /MPa	Poisson ratio
32	2.3	292.8	392.3	2.03×10^5	0.3
40	2.3	290.7	386.1	2.02×10^5	0.3

of the pipeline to make the pipelines of entire distance between anchorage points could expand when fault moves, as shown in Fig. 1. Using this method, the axial tension of the entire distance between anchorage points on pipelines, including large and small deformation sections, could be taken into account. This semi-rigid constraint makes the ends of pipe neither completely fixed nor freely expandable and can better simulate the actual interstation condition, as shown in Fig. 2.

2.2 Material properties

The soil in soil-box and pipe adopted clay and galvanized steel tube, respectively. The mechanical properties of clay were measured by unconsolidated undrained triaxial compression test, as presented in Table 2. The tensile test was carried out on the pipeline, and the mechanical properties are measured, as listed in Table 3.

2.3 Layout of measuring points

Eighteen strain gauges were symmetrically bonded along the pipeline axis to measure the strain distribution of the pipeline, as shown in Fig. 3. The strain acquisition system adopted was DH3816 static strain acquisition instrument, as shown in Fig. 4(b). Due to the small diameter of the pipe selected in the test, the accurate attach positions ware marked and the surfaces of them were cleaned with

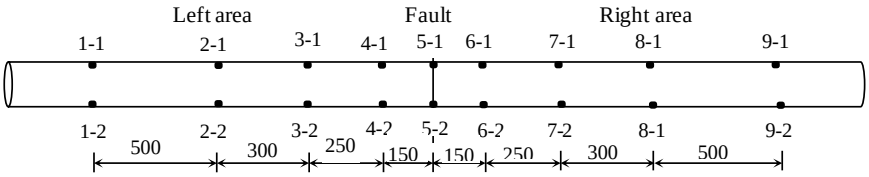

Fig.3. Strain gauge arrangement.

Table 4 The schematics of three types of faults

Normal fault	Strike-slip fault	Oblique slip fault
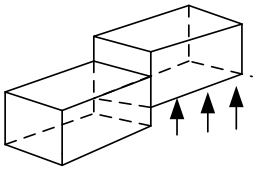	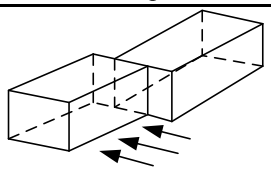	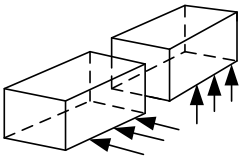

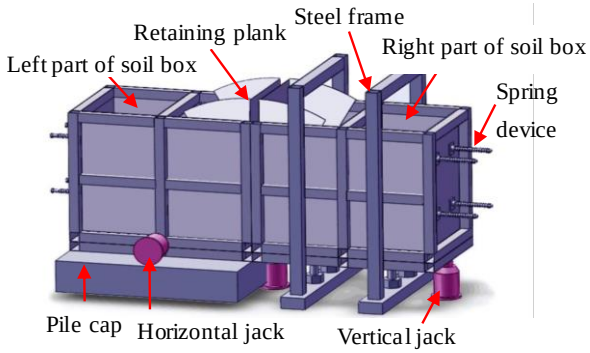

(a) Self-made soil-box device

(b) Strain measurement system

Fig. 4 Loading and measuring device

alcohol before the strain gauges were mounted with epoxy resin. Each of the attached gauges was covered with a circle of tape for protection, and tested with ohmmeter every time before the experiment.

2.4 Test loading

As shown in Fig. 4(a), a self-made soil-box, with the dimension of 3.0 m (length) × 1.0 m (width) × 1.1 m (height), was utilized in the test. The fault crossing angle and fault dip angle in the test are both 90°. The vertical and horizontal displacements, which could both range from 0 mm to 140 mm with an increment of 10mm, were controlled by hydraulic jacks. The horizontal displacement of the left part of the soil-box was exerted by the horizontal jack, and the vertical displacement of the right part was exerted by the vertical jacks. When simulating normal fault, the left part of soil-box was fixed and the right part of soil-box moved vertically under the action of vertical jacks; when simulating strike slip fault, the right part of soil-box was fixed and the left part of soil-box moved horizontally under the action of horizontal jack; when simulating oblique slip fault, the left jack and right jack worked simultaneously to exert displacement on both the left and right part of the soil-box. The schematics of three types of faults were presented in Table 4.

3. Test results and discussion

3.1 Deformation modes

Figs. 5(a)-(c) show the soil deformation under the normal fault, the strike-slip fault and the oblique-slip fault, respectively. Comparing these three figures shows that a crack appears at the fault and approximately parallel to it, while the soil far from the fault has no obvious deformation. However, in Fig. 5(a), the surface of the soil near the fault is uplifted and the crack at the fault is wider. In Fig. 5(b), there is no obvious uplift on the soil surface near the fault, and the crack at the fault is narrow. In Fig. 5(c), the soil surface near the fault is uplifted and severely damaged, and the crack at the fault is the largest. Pipelines deform with the movement of the fault constrained by the surrounding soil, and the deformation is consistent with the fault displacement. The deformation of the pipeline after loading were shown in Fig. 5(d). Comparing the deformation of N-32-0.3, S-32-0.3 and O-32-0.3, it can be seen that the pipeline deformation is the largest in the case of the oblique slip fault. Comparing the deformation of N-32-0.3, N-32-0.6 and S-32-0.3, S-32-0.6, respectively, it can be seen that the deformation of pipelines decreases with decreasing buried depth or increasing pipe diameter. Fig. 5 (d) shown that the buried pipelines crossing the normal fault and the

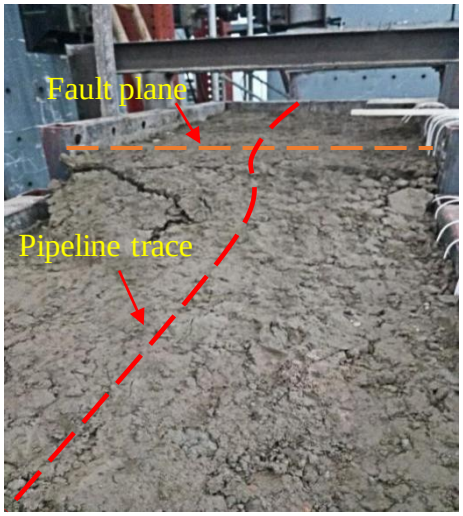

(a) Soil deformation under the normal fault

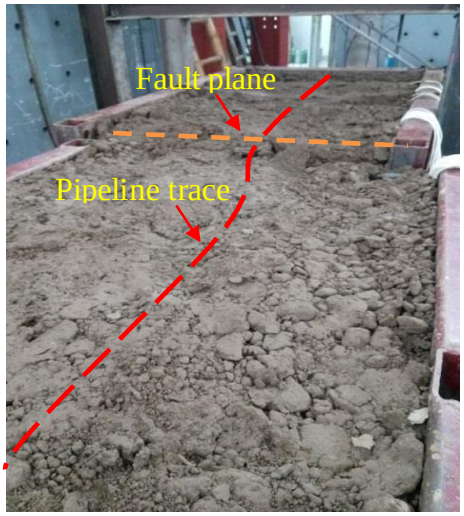

(b) Soil deformation under the Strike-slip fault

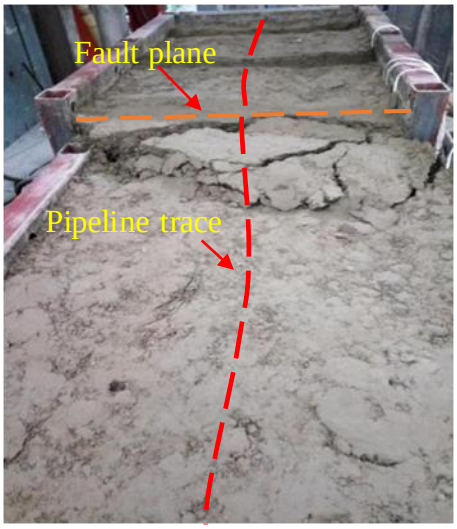

(c) Soil deformation under the oblique slip fault

(d) Pipelines deformation

Fig. 5 Deformation of soil and pipelines

*Notes: the pipelines in Fig. 5(d) are hollow pipelines, the relevant parameters were provided in Table 1

oblique fault experienced asymmetric deflection around the fault plane, of which the reason was that the vertical uplift and vertical bearing soil reaction were different. For buried pipelines crossing the strike-slip fault, the pipelines experienced relatively similar deflection around the fault plane, for the horizontal soil reaction on the pipeline were relatively consistent.

3.2 Axial strain

3.2.1 Influence of fault displacement

The axial strains of measuring points under different fault displacements are shown in Fig. 6, in which the yield strain of pipe material was marked with dash line in red to reveal the pipeline's behavior beyond the elastic zone. Taking N-32-0.3, S-32-0.3 and O-32-0.3 as examples to analyze the influence of fault displacement on the axial strain of pipeline. Comparing Fig. 6(a) with Fig. 6(b) shows that in case of the normal fault, the axial strain of all measuring point has an upward trend when the fault displacement is gradually increased from 0mm to 140mm, and furthermore, a smaller peak strain appears at the measuring points 5-1, 5-2 at the fault and the measuring points 1-1, 1-2, 9-1, 9-2 far from the fault. Additionally, when the fault displacement is 140 mm, the axial tensile and compressive peak strain on the upper side of the pipeline appear at the measuring points 2-1 and 8-1, respectively. However, those on the lower side appear at the measuring points 2-2 and 8-2, respectively. The measuring points from 6-1 to 9-1 on the upper side of the pipeline in the right part of soil-box are subjected to tension, while the measuring points from 6-2 to 9-2 on the lower side of the pipeline are compressed. Conversely, the measuring points from 1-1 to 4-1 on the upper side of the pipeline in the left part of soil-box are compressed and the measuring points from 1-2 to 4-2 on the lower side is subjected to tension. The axial Tensile and compressive peak strain of the pipeline is about 700 mm away from the fault. From Figs. 6(c)-(f) reveal that the pipelines under the strike-slip fault and the oblique-slip fault have similar trends. It can be

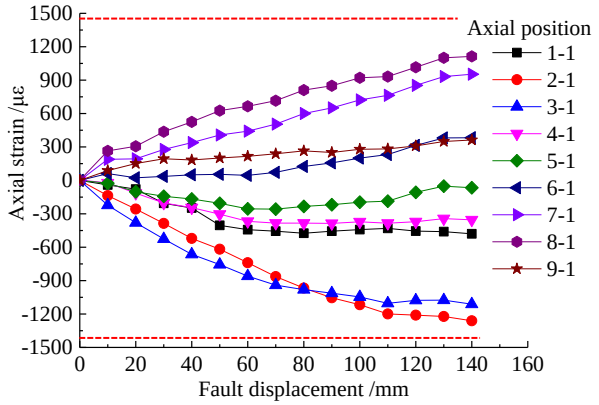

(a) Upper side axial strain of N-32-0.3

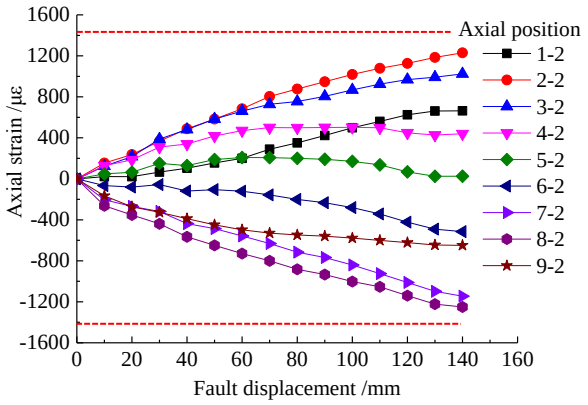

(b) lower side axial strain of N-32-0.3

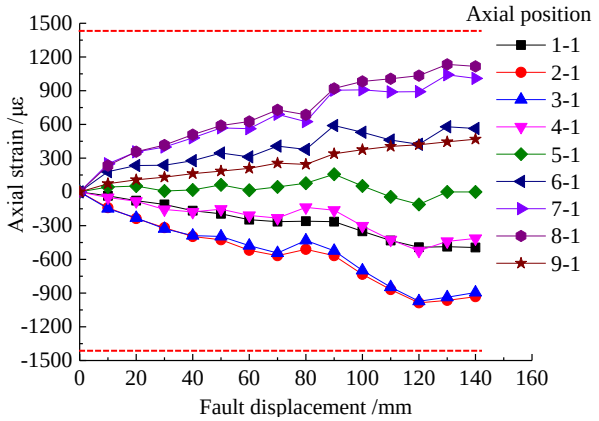

(c) Left side axial strain of S-32-0.3

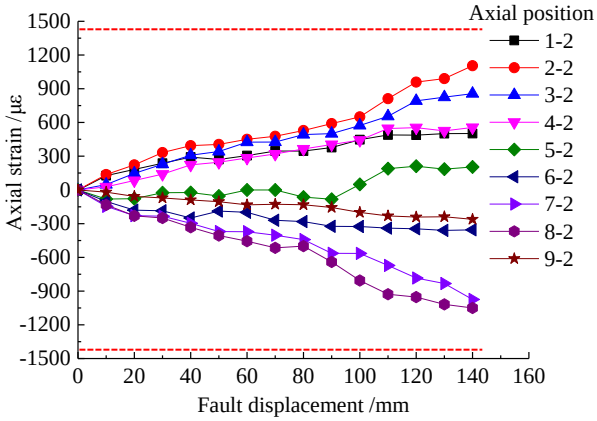

(d) Right side axial strain of S-32-0.3

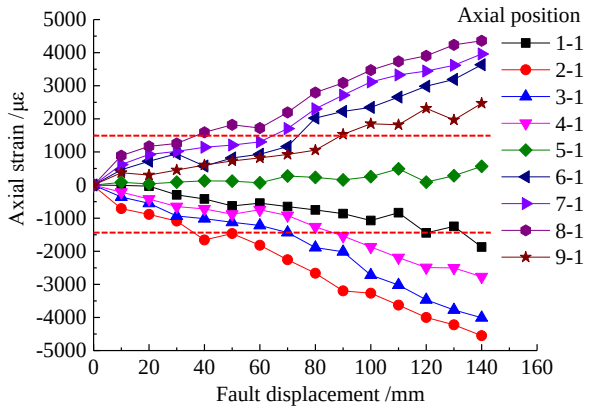

(e) Left upper side axial strain of O-32-0.3

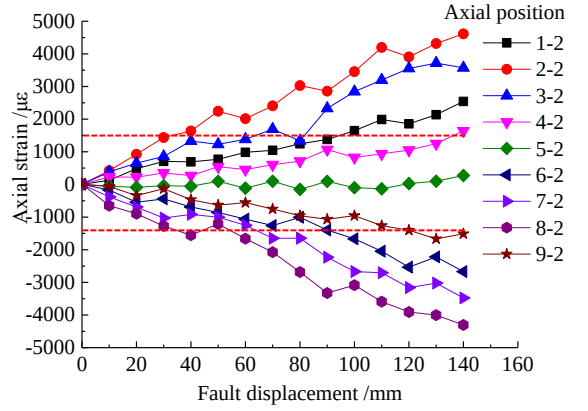

(f) Lower right side axial strain of O-32-0.3

Fig. 6 Axial strain of specimens under different fault displacement

concluded that the axial strain of different measuring points increase with increasing fault displacement. The peak strain is not at the fault, but near the two sides of the fault.

3.2.2 Influence of buried depth

The axial strain distribution under different buried depth was shown in Fig. 7 with the selection of 0.3m and 0.6m buried depth to analyze the influence of buried depth on the axial strain of the buried pipeline crossing fault. In the case of the normal fault, specimen N-32-0.3 and specimen N-32-0.6 were taken as examples for analysis. The axial strain distribution of N-32-0.3 and N-32-0.6 were shown in Figs. 7(a)-(d), respectively. It shown that the axial peak strain of the pipeline is not at the fault, but near the two sides of the fault. The upper side of the pipeline in the left part of the soil-box was compressed and the lower side was subjected to tension, while the upper side of the pipeline in the right part of the soil-box is subjected to tension and the lower side is compressed. It can be seen from the figures that the axial strain distribution of the upper sides and lower sides of the pipeline is asymmetrical along the fault plane, due to the difference between the vertical uplift and vertical bearing soil reaction. When the buried depth is 0.3m, the axial tensile peak strain of the pipeline is always greater than that

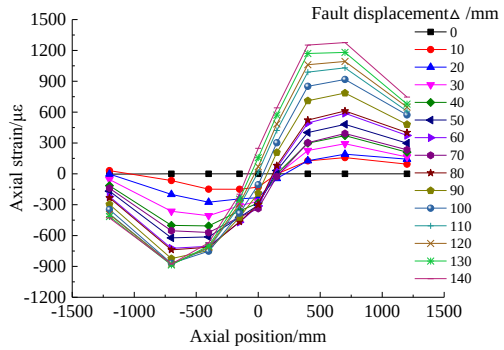

(a) Upper side axial strain of N-32-0.3

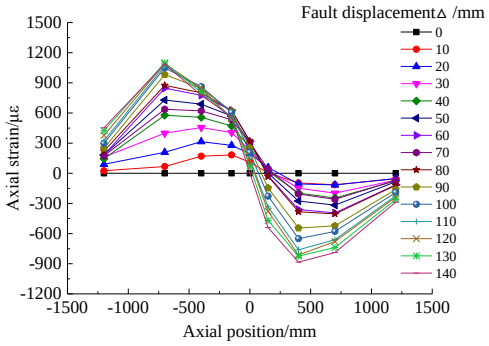

(b) Lower side axial strain of N-32-0.3

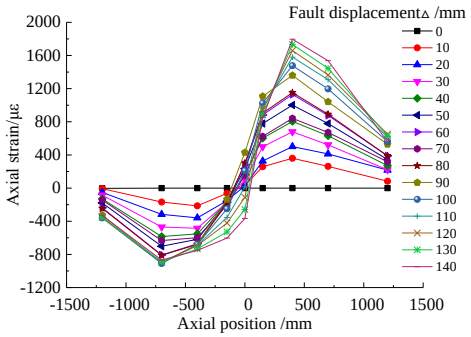

(c) Upper side axial strain of N-32-0.6

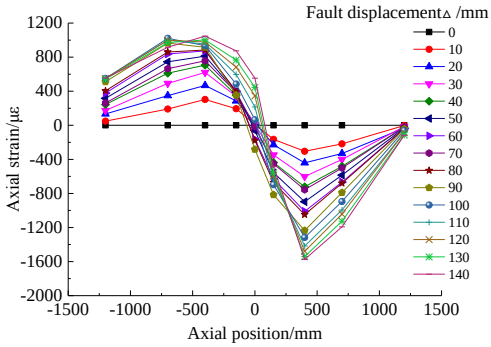

(d) Lower side axial strain of N-32-0.6

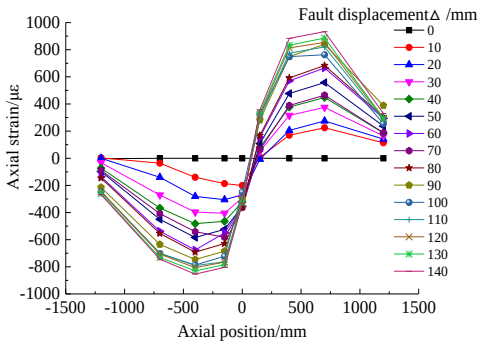

(e) Upper side axial strain of N-40-0.3

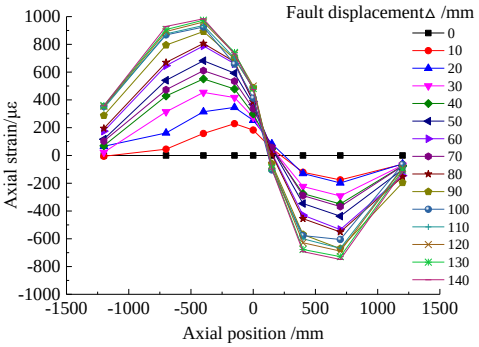

(f) Lower side axial strain of N-40-0.3

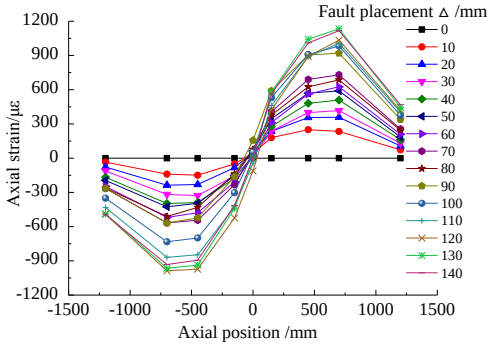

(g) Left side axial strain of S-32-0.3

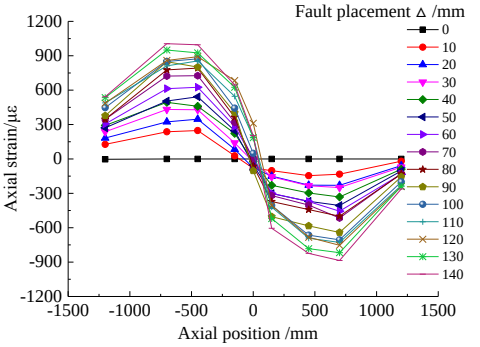

(h) Right side axial strain of S-32-0.3

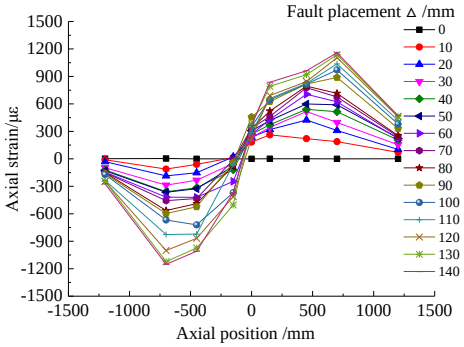

(i) Left side axial strain of S-32-0.6

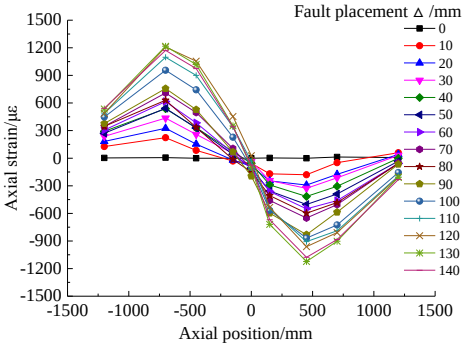

(j) Right side axial strain of S-32-0.6

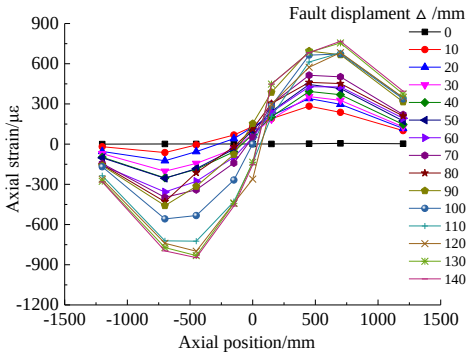

(k) Left side axial strain of S-40-0.3

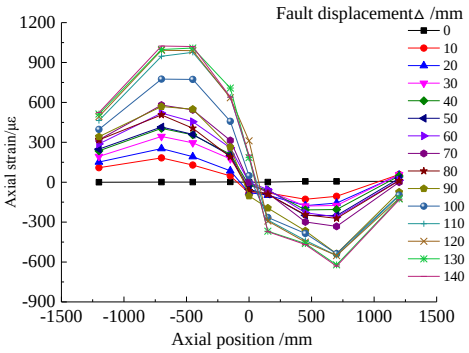

(l) Right side axial strain of S-40-0.3

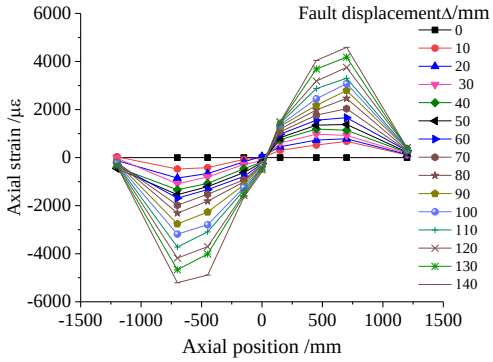

(m)Left upper side axial strain of O-32-0.3

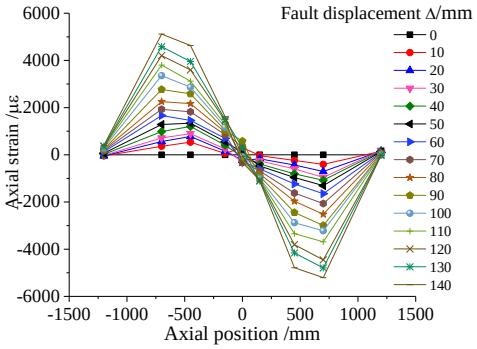

(n)Lower right side axial strain of O-32-0.3

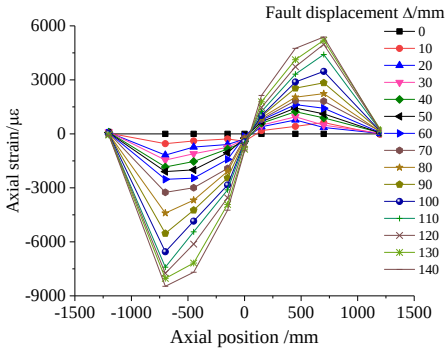

(o)Left upper side axial strain of O-32-0.6

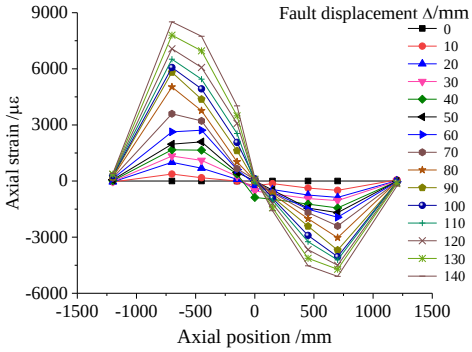

(p)Lower right side axial strain of O-32-0.6

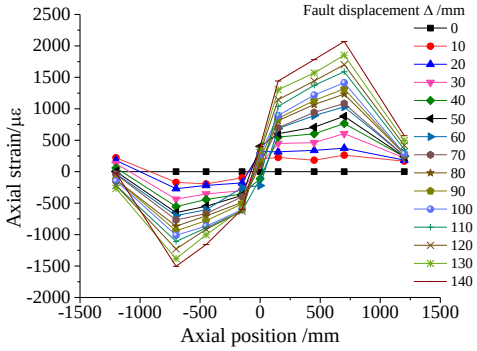

(q)Left upper side axial strain of O-40-0.3

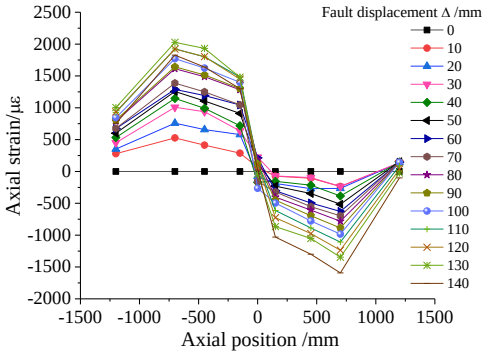

(r)Lower right side axial strain of O-40-0.3

Fig.7 Axial strain distribution of specimens

of the compressive peak strain. Therefore, the pipeline is mainly subjected to tension. When the buried depth is 0.6m, the axial peak strains of pipeline on the left side and right side of fault are around 900με and 1600με, respectively. It can be seen that with the increase of buried depth, the upper side of the pipe is mainly subjected to tension, the lower side is mainly compressed, and the axial strain distribution of the upper sides and lower sides of the pipeline is asymmetrical along the fault plane. Comparing the axial strain of the upper side and lower side of the pipeline, the

axial tensile and compressive peak strain on the both sides of the pipeline with a depth of 0.6m are larger than those of the pipeline with a depth of 0.3m. From Figs. 7(g)-(j), despite the difference of buried depth, the axial strain distribution in the left and right parts of the pipeline is approximately symmetric along the fault plane in the case of strike-slip fault. From Figs. 7(m)-(p), the left upper side of the pipelines is compressed and the lower right side of the pipelines is subjected to tension in the case of oblique-slip fault. Additionally, the axial strain of pipeline crossing strike-slip fault and oblique slip fault increases with increasing buried depth, similar with that of normal fault. Therefore, it is concluded that the axial peak strain of the pipeline emerges on the two sides of the fault, rather than the fault itself, and the restraint action of pipe-soil and the axial strain response of pipeline increases with the increasing buried depth. A shallow burial is beneficial to resisting the fault movement of a pipeline.

3.2.3 Influence of the ratio of pipe diameter to pipe wall thickness

The ratios of pipe diameter to pipe wall thickness with a diameter of 32mm and 40mm are 13.91 and 17.39, respectively. The axial strain distribution under different ratios of pipe diameter to pipe wall thickness is shown in Fig.7. From Figs. 7(a)-(b) and Figs. 7(e)-(f), it can be seen that in case of normal fault, the axial strain distribution of the upper side of the pipeline is asymmetrical along the fault plane, so is the lower side. The symmetrical center of the strain curve of N-40-0.3 is offset, the reason is that the pipe-soil restraint action increases with increasing ratios of pipe diameter to pipe wall thickness or decreasing displacement. The axial tensile and compressive peak strain of N-40-0.3 are around 700με and 900με, respectively. While those of N-32-0.3 are around 1200με. It can be known that cross section moment of inertia increases with increasing ratio of pipe diameter to pipe wall thickness, it also increases the stiffness of the pipeline and enhances the restraint action of the pipe-soil. When fault displacement gradually increases to 140 mm, the reason why the pipe stiffness can always resist the pipe-soil restraint is the pipe diameter increases. From Figs. 7(g)-(h), Figs. 7(k)-(l) and Figs. 7(m)-(n), and Figs. 7(q)-(r), it can be seen that the axial strain of pipelines crossing strike slip fault and oblique slip fault decreases with increasing ratio of pipe diameter to pipe wall thickness, the same as that of the crossing normal fault. Therefore, it is concluded that the axial strain of the pipeline decreases with increasing ratio of pipe diameter to pipe wall thickness. For design of pipeline crossing fault, the influence of ratio of pipe diameter to pipe wall thickness should be considered.

3.2.4 Influence of fault type

When the angle between the pipeline and normal fault is 90°, the axial strain distribution of the pipeline is shown in Figs. 7(a)-(f). It can be seen that the axial strain distribution of the upper side of the pipeline is asymmetrical along the fault plane, so is the lower side. The reason is that the vertical uplift and vertical bearing soil reaction is difference. The soil restraint plays a leading role when the fault displacement is small. However, the symmetrical center of the strain curve is offset after the fault displacement reaches to 60 mm, the reason is that the pipe-soil restraint action is weakens with the increasing fault displacement, the fault displacement plays a dominant role.

When the angle between the pipeline and strike-slip fault is 90°, the axial strain distribution of the pipeline is shown in Figs. 7(g)-(l). It shown that a few strain curves are offset, the reason is that the soil restraint on the pipeline plays a leading role when the fault displacement is small. The axial strain distribution of the left and right areas of the pipeline is approximately symmetric along the fault plane, the reason is that the horizontal soil action on the pipeline are relatively consistent. From Figs. 7(k)-(l), it can be seen that are some differences in the axial strains on both sides of the fault, the reason is that the soil surrounding pipelines is not homogenous at both sides of the fault. The pipeline is also subjected to similar reaction force when the fault displacement is increase.

When the angle between the pipeline and oblique slip fault is 90°, the axial strain distribution of pipeline is shown in Figs. 7(m)-(r). Similar to normal faults and strike-slip faults, in case of oblique slip fault, the axial strain increases with the increase of burial depth and the decrease of diameter. Comparing the peak strain in Figs. 7(a)-(r), thus it is clear that oblique slip fault has the greatest damage to pipelines, followed by normal fault, while strike slip fault has the least damage. Additionally, the axial strain distribution of the left upper side of the pipeline is asymmetrical along the fault plane, so is the lower right side. The reason is that the vertical uplift and vertical bearing soil reaction is difference.

4. Finite element analysis (FEA) mode

To further investigate the mechanical behavior of buried pipeline crossing fault, a three-dimensional FEA model was developed.

4.1 Finite element type and mesh

The FEA model was divided into two parts: the soil and the pipeline made from steel tube. According to references (Du *et al*. 2018a, Du *et al*. 2018b), the four nodes shell elements with reduced-integration (S4R) was selected for simulating the steel pipeline while the eight nodes brick solid elements with reduced-integration (C3D8R) was used for simulating the soil. Mesh generation adopted the structural meshing technology to obtain more regular hexahedron elements. This model focused on the large deformation section of pipelines, so the meshes of soil and pipeline are refined within 500 mm from both sides of fault, as shown in Fig. 8 (a)

4.2 Material model

In consideration of material properties of clay, the ideal elastic-plastic Mohr-Coulomb model is used to simulate mechanical properties of soil, as shown in Fig. 9(a). It can

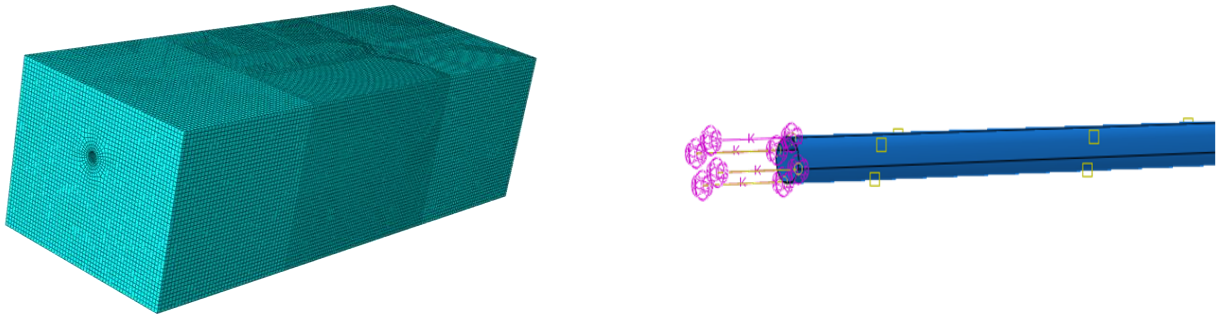

(a) Model meshing (b) Spring constraint

Fig. 8 Three-dimensional FEA model

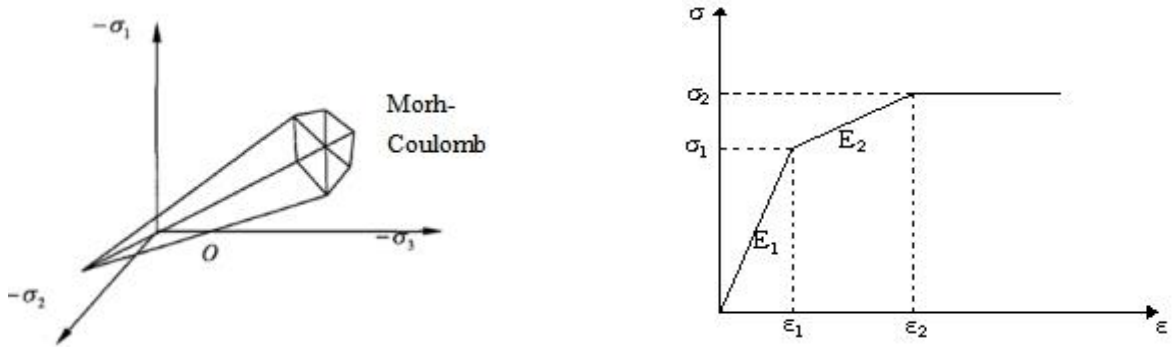

(a) Mohr-coulomb model of soil (b) trilinear line model of pipeline

Fig. 9 Material constitutive mode

be divided into two stages: elastic stage, elastic-plastic stage. The elastic stage is represented by Hooke's Law; Mohr-Coulomb yield criterion is used to analyze the elastic-plastic stage, the elastic modulus, density, Poisson's ratio and friction angle need to be input. The cohesion is also specified and the dilatancy angle is set to 0. The material properties of soil are shown in Table 2. In consideration of the elastic-plastic characteristics of the pipeline, the elastic-plastic model is used to simulate mechanical properties of pipeline. It can be divided into two parts: Elastic part, plastic part. The elastic part needs to input elastic modulus and Poisson's ratio; the plastic part needs to input the stress-strain curve obtained from the tensile test. The trilinear line model was adopted by the pipeline, which can be divided into three stages: elastic stage, elastic-plastic stage and plastic stage, as shown in Fig. 9(b), where ε_1, ε_2, σ_1 and σ_2 represent elastic yield strain, plastic yield strain, elastic yield stress and plastic yield stress of the pipeline, respectively; E_1 and E_2 denote the material modulus of pipeline at elastic deformation stage and stress strengthening stage, respectively. The mechanical properties of pipeline are shown in Table 3.

4.3 The contact between soil and pipeline

When analyzing the buried pipeline under the fault displacement, the force is transmitted by contact between soil and pipeline. The non-linearity of contact interface will be involved when the pipeline interacts with the soil. This paper selects the surface-to-surface contact algorithm to define the interaction of pipeline and soil. It can be divided into two parts: tangential action is defined by the Coulomb friction model; normal action is defined by hard contact. In the finite element method, the rigid object is regarded as the main control surface, the object with less rigidity acts as a subordinate surface. Due to the rigidity of the pipeline, the outer wall of the pipeline selection as the main control surface, soil surface as a dependent.

4.4 Boundary conditions and load application

In the FEA, the boundary conditions are set as follows: the upper surface of the model is the ground surface, and there is no need to add boundary conditions. Under normal faults, displacement constraints and angle constraints in X, Y and Z directions are applied to the bottom surface of the fixed end, and corresponding displacement loads are applied to the bottom surface of the moving end. The front and posterior surfaces and the left and right surfaces are only constrained by displacement in the X direction. Under strike-slip faults, displacement and angle constraints in X, Y and Z directions are applied to the bottom surface of the fixed end. The displacement constraints in the direction of X and Y are applied to the front and posterior surfaces of the fixed end, while the displacement constraints in the direction of Y are applied only to the front and rear surfaces of the moving end. Under the oblique fault, the boundary conditions and displacement loads of normal faults and strike-slip faults need to be considered comprehensively. In the model, the displacement loading method is adopted to

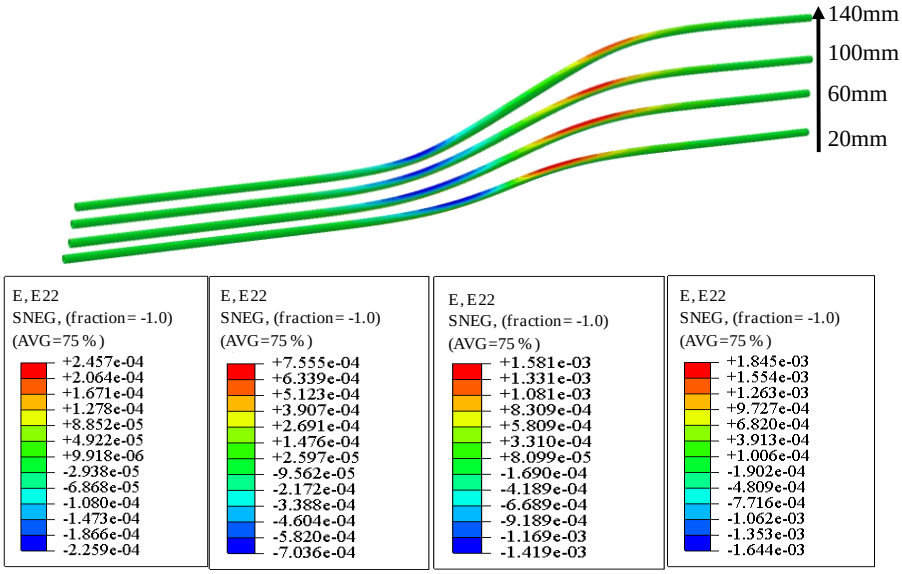

(a) Normal fault

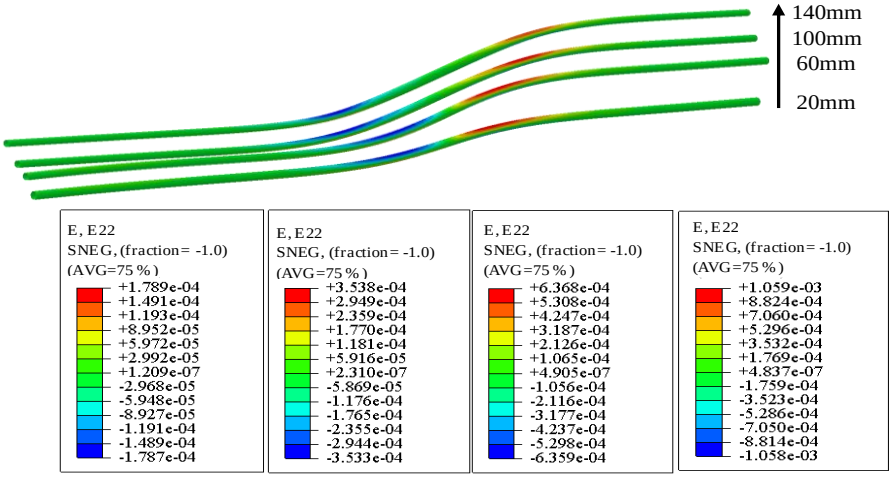

(b) Strike-slip fault

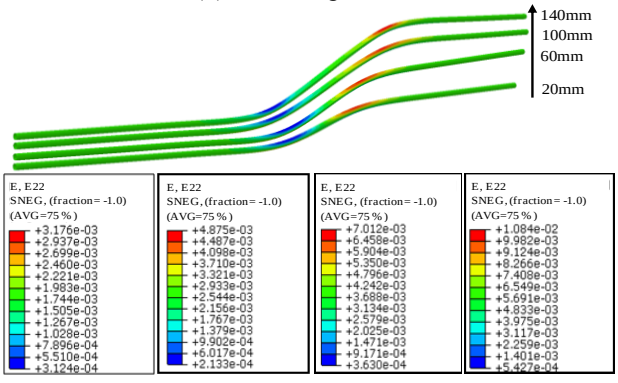

(c) Oblique slip fault

Fig. 10 Strain nephogram along the pipeline axis

simulate the influence of different types of fault displacement on the mechanical performance of the buried pipeline. It is achieved by applying displacement on the bottom or side of the moving end. Because of the end of the pipeline is connected by spring device, the end constraint is established by selecting the spring element and determining the spring elastic coefficient, as shown in Fig.8 (b).

5. Comparison between the predicted and experimental results

5.1 Deformation mode

The axial strain nephograms of specimens N-32-0.3, S-32-0.3 and O-32-0.3 under different fault displacement are

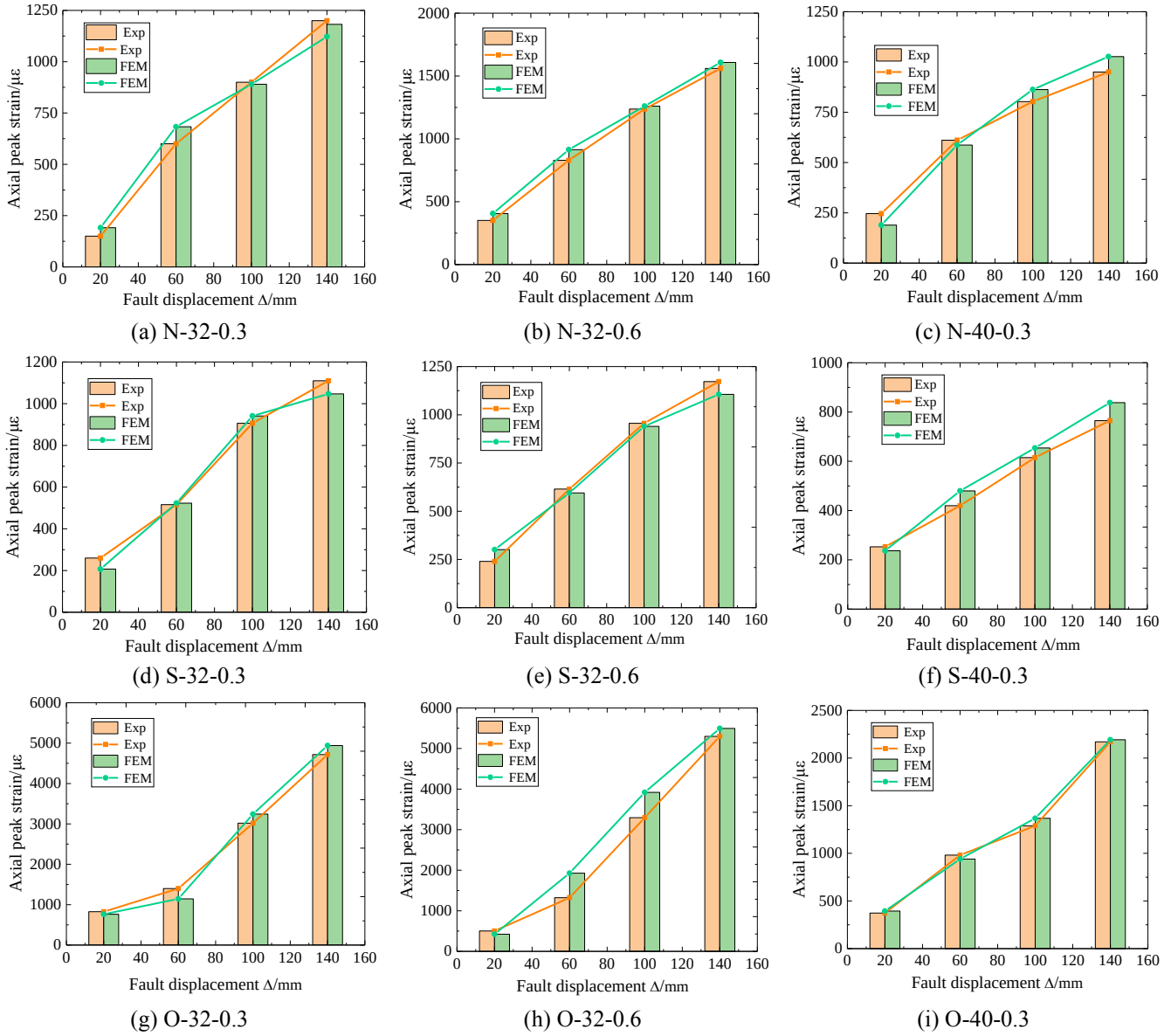

(a) N-32-0.3 (b) N-32-0.6 (c) N-40-0.3

(d) S-32-0.3 (e) S-32-0.6 (f) S-40-0.3

(g) O-32-0.3 (h) O-32-0.6 (i) O-40-0.3

Fig. 11 Comparisons of peak axial strains between the predicted results in FEA and measured results in test (Exp)

Table 5 The maximal differences between the FEA results and Exp results

Specimen	Fault displacement/mm	Measured results /με	Predicted results/με	Maximal differences
N-32-0.3	60	644	683	5.710%
N-32-0.6	20	379	403	5.955%
N-40-0.3	20	231	213	7.792%
S-32-0.3	20	232	213	8.190%
S-32-0.6	20	248	274	9.489%
S-40-0.3	60	427	471	9.342%
O-32-0.3	60	1379	1275	7.542%
O-32-0.6	60	1638	1808	9.403%
O-40-0.3	100	1291	1349	4.299%

shown in Figs. 10(a)-(c). It can be seen that the FEA and the experimental pipeline deformation have similar results. The maximum deformation of the pipeline is not at the fault, however near the fault. With the increase of the fault displacement, the deformation and strain of pipeline increase. From Figs. 10(a)-(c), it can be found that the FEA results are in good agreement with the experimental results: the oblique slip fault has the greatest influence on the axial

Table 6 Parameters design of model

No.	*t*/mm	*D*/mm	*d*/mm	Δ /mm	*L*/mm
1	10	300	300	200	30000
2	15	400	600	400	30000
3	20	500	900	600	30000
4	25	600	1200	800	30000
5	30	700	1500	1000	30000

*Notes: *t, D, d,* Δ *and L* denotes wall thickness, diameter, buried depth, fault displacement and length of the pipeline respectively.

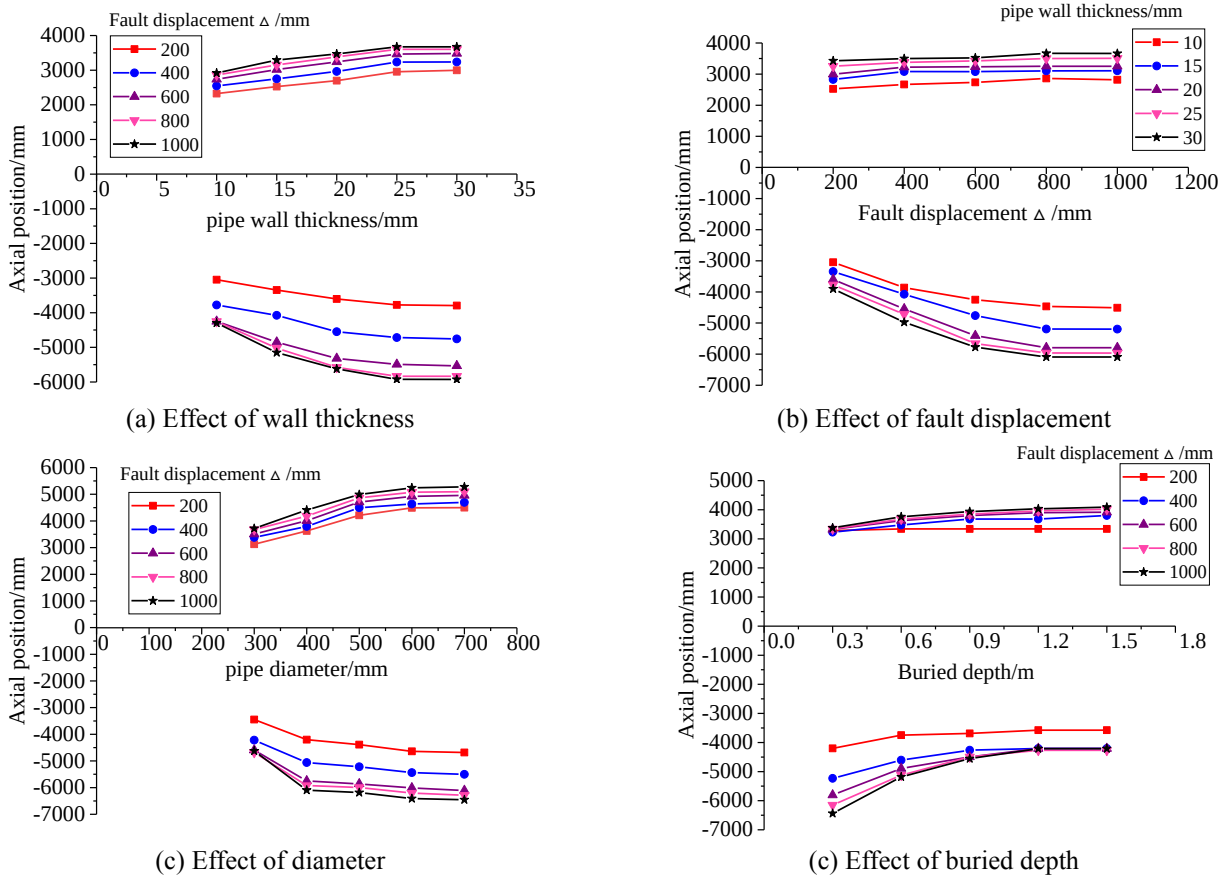

(a) Effect of wall thickness

(b) Effect of fault displacement

(c) Effect of diameter

(c) Effect of buried depth

Fig. 12 The variation trend of the axial distance from the peak axial strain position of the pipeline to the fault under the effects of different parameters

strain and deformation of buried pipelines in case of the same fault displacement, followed by the normal fault, while the strike slip fault has the least influence. Fig. 10 shows that the buried pipelines crossing the normal fault and the oblique fault experienced asymmetric deflection around the fault plane. For the case of buried pipelines crossing the strike-slip fault, it is observed that the pipelines experienced relatively similar deflection around the fault plane

5.2 Axial peak strain

For the buried pipelines under fault movement, their peak axial strains at the measuring points 8-1 predicted in FEA were compared with the measured results (Exp) in test, as shown in Fig. 11. It is clear that the FEA results agree well with the experimental (Exp) results. It is also clear from Fig.11 that the peak axial strain predicted in FEA and measured values of test increase with increasing fault displacement. Additionally, from Figs. 11(a)-(b), under the normal fault, the peak axial strain predicted by FEA increases with the buried depth, which agrees with the trends from the experiment. The similar conclusion can be draw when the buried pipeline under the strike-slip fault and oblique slip fault by comparing Fig.11(d) with Fig. 11(e) and Fig. 11(g) with Fig. 11(h), respectively. Under the strike-slip fault, Figs. 11(d)-(f) reveal that, influenced by the ratios of pipe diameter to pipe wall thickness, the changing trends of the numerical peak axial strain and experimental values are the same. The axial peak strain increases with

decreasing ratios of pipe diameter to pipe wall thickness. The respective comparison of Fig. 11(a) with Fig. 11(c) and Fig. 11(g) with Fig. 11(i) show that there is a similar conclusion under the normal fault and oblique slip fault. As can be seen from Fig. 11(b), Fig. 11(e) and Fig. 11(h), in the finite element analysis, the influence of fault type on the peak axial strain of pipeline is the same as that obtained from the test. The oblique slip fault has the greatest impact on the pipeline strain, followed by the normal fault, while the strike-slip fault has the least influence.

5.3 The regression equations of the position of peak axial strain

The experimental results are in good agreement with the FEA results. Based on the accuracy of the finite element model, four parameters were selected to study the variation trend of the axial distance from the peak axial strain position of the pipeline to the fault in large deformation section under normal fault, Parameters design shown in Table 6. The effects of wall thickness, fault displacement and diameter on the axial distance from the peak axial strain position of the pipeline to the fault were shown in Fig. 12(a), Fig. 12(b) and Fig. 12(c) respectively. It can be seen that the axial distance from the peak axial strain position of the pipeline to the fault increases with increasing wall thickness, diameter and fault displacement. However, as shown in Fig. 12(d), the axial distance from the peak axial compressive strain position of the pipeline to the fault decreases with increasing buried depth, the axial distance of tensile side increases with increasing buried depth.

Based on the analysis of the above-mentioned working conditions, the regression equations of the position of peak axial strain of pipeline crossing normal fault to the axial distance of fault are given under the effects of various parameters.

The axial distance from the peak axial tensile strain position of the pipeline to the fault:

$$y = 0.97t^2 + 4.33D + 0.52\Delta + 0.67d + 866.3 \quad (1)$$

The axial distance from the peak axial compressive strain position of the pipeline to the fault:

$$y = 0.001t^4 + 5.9\times10^{-6}D^3 + 0.0015\Delta^2 - 0.58d + 3900 \quad (2)$$

"t" represents the wall thickness, mm. "D" represents the pipeline diameter, m. "d" represents buried depth, mm. "Δ" represents fault displacement, mm.

The results of the regression equation are fitted with the consequences of the finite element model (FEM), which indicates a high degree of fitting as can be drawn from Figure 13. The regression equation can simplify the analysis of peak strain position of pipeline and provide a reference for the study of buried pipelines crossing faults.

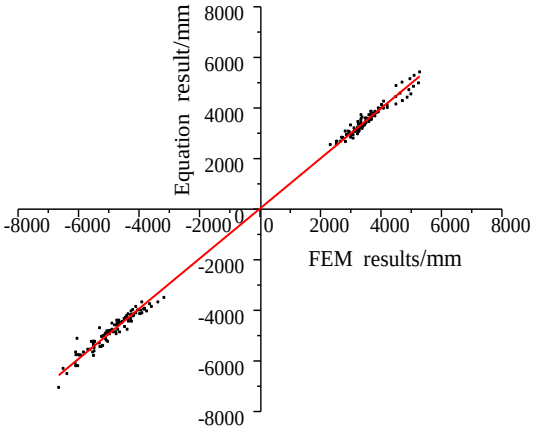

Fig. 13 Comparison of regression equation results with the FEM results

6. Discussion of future work

In this paper, only the mechanical properties of healthy pipelines under fault movements are analyzed, however, in service pipelines often have pre-existing damages. Therefore, a pipeline with pre-existing damages should be considered in the future research, and the mechanical properties of the damaged buried pipeline under fault movements should be explored. Besides, when studying the axial distance from the peak of the pipeline strain to the fault, a preliminary study was performed with finite element analysis alone resulting in a regression equation, yet parameters related to soil and relative soil -pipe stiffness were not considered in the regression analysis. Thus, parameters related to soil and relative soil -pipe stiffness should be considered in the future research of buried pipelines crossing faults. As demonstrated in this research, fault movements deform a pipeline and possibly cause damages to the pipeline, therefore, it is important to perform real-time health monitoring of the pipeline. A potential candidate to perform health monitoring of a pipeline subject to fault movement is the piezoceramic transducer (Tian *et al*. 2019) along with the supporting algorithms. However, the use of piezoceramics to detect real-time damage of the buried pipeline subject to fault movement has not been studied in this paper. The future research will use transducers made of the PZT (Lead Zirconate Titanate), a type of piezoceramic material with strong piezoelectric effect, to monitor real-time damage of buried pipeline across a fault. The future research will continue to use the soil-box scale test model with the equivalent spring boundary.

7. Conclusions

This paper studied the mechanical behavior of buried pipelines crossing faults by experimental and numerical methods. The major findings of the research are summarized in the following:

- The axial strain at different measuring points of the buried pipelines crossing faults increases with increasing fault displacement. The axial peak strain appears near both sides of the fault, while the strain at the fault and at the farther measuring points are relatively small.
- The pipe-soil restraint action and the axial strain

increases with increasing buried depth. Increasing the ratio of pipe diameter to pipe wall thickness is beneficial for pipeline to resist fault displacement and decrease the axial strain of the pipeline.

• Compared with a normal fault and a strike-slip fault, the axial strain response of the pipeline under an oblique slip fault is the largest, Therefore, the oblique fault has the greatest harm to the pipelines.

• For pipelines crossing the normal fault and the oblique fault, the deformation and axial strain distribution of pipelines are asymmetric along the fault plane. However, for the case of buried pipelines crossing strike-slip faults, the deformation and axial strain distribution of pipelines are approximately symmetric along the fault plane if the soil surrounding pipelines is homogenous at both sides of the fault plane.

• For a normal fault, the axial distance from the peak axial strain position of the pipeline to the fault increases with increasing wall thickness, diameter and fault displacement. However, the axial distance from the peak axial compressive strain position of the pipeline to the fault decreases with increasing buried depth, and the axial distance of tensile strain position increases with increasing buried depth. The regression equation can simplify the peak axial strain position analysis and provides a reference for the study of buried pipelines crossing faults.

Acknowledgments

The research presented in this paper is part of Project (51778064) supported by Natural Science Foundation of China, the Project (2016D-5007-0605) supported by Petroleum Science and Technology Innovation Foundation of China, and the Project (2016CFA022) supported by Natural Science Foundation of Hubei Province, China. The financial support is highly appreciated.

References

Arafah, D., Madia, M., Zerbst, U., Beretta, S. and Cristea, M.E. (2015), "Instability analysis of pressurized pipes with longitudinal surface cracks", *J.Pressure Vessels Piping*, **126**, 48-57. https://doi.org/10.1016/j.ijpvp.2015.01.001.

Arzaghi, E., Abaei, M.M., Abbassi, R., Garaniya, V., Chin, C. and Khan, F. (2017), "Risk-based maintenance planning of subsea pipelines through fatigue crack growth monitoring", *Eng. Failure Anal.*, **79**, 928-939. https://doi.org/10.1016/j.engfailanal.2017.06.003.

ASCE (1984), *Guidelines for the Seismic Design of Oil and Gas Pipeline Systems*, American Society of Civil Engineers, New York, USA.

Audibert, J.M.E. and Nyman, K.J. (1977), "Soil restraint against horizontal motion of pipes", *J. Geotech. Eng. Division*, **103** (10), 1119-1142.

Cheng, X.D., Ma, C., Huang, R.K., Huang, S.N., Yang, W.D. (2019), "Failure mode analysis of X80 buried steel pipeline under oblique-reverse fault", *Soil Dynam,. Earthq. Eng.*, **125**,105723. https://doi.org/10.1016/j.soildyn.2019.105723.

Cocchetti, G., Di Prisco, C. and Galli, A. (2008), "Soil-pipeline interaction along active fault systems", *J. Offshore Polar Eng.*, **18**(3), 211-219.

Dong, F.F., Bie, X.M., Tian, J.P., Xie, X.D., Du, G.F. (2019), "Experimental and numerical study on the strain behavior of buried pipelines subjected to an impact load", *Appl. Sci.-Basel,* **9**(16), 3284. https://doi.org/10.3390/app9163284.

Du, G.F., Andjelic, A., Li, Z., Lei, Z. and Bie, X.M. (2018b), "Residual Axial Bearing Capacity of Concrete-Filled Circular Steel Tubular Columns (CFCSTCs) after Transverse Impact", *Appl. Sci*., **8**(5), 793. https://doi.org/10.3390/app8050793.

Du, G.F., Babic, M., Wu, F.H., Zeng, X. and Bie, X.M. (2018a), "Experimental and Numerical Studies on Concrete Filled Circular Steel Tubular (CFCST) Members Under Impact Loads", *J. Civil Eng.*, **17**(8A), 1211-1226. https://doi.org/10.1007/s40999-018-0379-8.

Du, G.F., Huo, L.S., Kong, Q.Z. and Song, G.B. (2016b), "Damage detection of pipeline multiple cracks using piezoceramic transducers", *J. Vibroeng.*, **18**(5), 2828-2838. https://doi.org/10.21595/jve.2016.17040.

Du, G.F., Kong, Q.Z., Lai, T. and Song, G.B. (2013), "Feasibility Study on crack detection of pipelines using piezoceramic transducers", *J. Distributed Sensor Networks*, **9**(10), 1-7. https://doi.org/10.1155/2013/631715.

Du, G.F., Kong, Q.Z., Zhou, H. and Gu, H.C. (2017), "Multiple cracks detection in pipeline using damage index matrix based on piezoceramic transducer-enabled stress wave propagation", *Sensors*, **17**(8), 1812.https://doi.org/10.3390/s17081812.

Du, G.F., Kong., Q.Z., Wu, F.H., Ruan, J.B. and Song, G.B. (2016a), "An experimental feasibility study of pipeline corrosion pit detection using a piezoceramic time reversal mirror", *Smart Mater. Struct.*, **25**(3), 037002. https://doi.org/10.1088/0964-1726/25/3/037002.

Erami, M.H., Miyajima, M., Kaneko, S., Toshima, T. and Kishi, S. (2015), "Pipe-soil interaction for segmented buried pipelines subjected to dip faults", *Earthq. Eng. Struct. Dynam.*, **44**(3), 403-417. https://doi.org/10.1002/eqe.2476.

Ha, D., Abdoun, T.H., O'Rourke, M.J., Symans, M.D., O'Rourke, T., Palmer, M.C. and Stewart, H.E. (2010), "Earthquake Faulting Effects on Buried Pipelines – Case History and Centrifuge Study", *J. Earthq. Eng.*, **14**(5), 646-669. https://doi.org/10.1080/13632460903527955.

Halabian, A.M. and Tohid, H. (2018), "A new hybrid model for rigorous analysis of buried pipelines under general faulting accounting for material and geometrical non-linearities with focusing on corrugated HDPE pipelines", *Soil Dynam. Earthq. Eng.*, **115**, 1-17. https://doi.org/10.1016/j.soildyn.2018.08.005.

Ho, M., El-Borgi, S., Patil, D. and Song, G.B. (2019), "Inspection and monitoring systems subsea pipelines: A review paper", *Struct. Health Monitor.*, https://doi.org/10.1177/1475921719837718.

Hou, Q.M., Jiao, W.L., Ren, L., Cao, H.Z. and Song, G.B. (2014), "Experimental study of leakage detection of natural gas pipeline using FBG based strain sensor and least square support vector machine", *J. Loss Prevention Process Industries*, **32**, 144-151. https://doi.org/10.1016/j.jlp.2014.08.003.

Jalali, H.H., Rofooei, F.R., Attari, N.K.A. and Samadian, M. (2016), "Experimental and finite element study of the reverse faulting effects on buried continuous steel gas pipelines", *Soil Dynam. Earthq. Eng.*, **86**, 1-14. https://doi.org/10.1016/j.soildyn.2016.04.006.

Jia, Z.G, Ren. L., Li, H.N., Jiang, T. and Wu, W.L. (2018a), "Pipeline leakage identification and localization based on the fiber Bragg grating hoop strain measurements and particle swarm optimization and support vector machine", *Struct. Control Health Monitor.*, **26**(2), e2290. https://doi.org/10.1002/stc.2290.

Jia, Z.G, Ren. L., Li, H.N., Wu, W.L. and Jiang, T. (2018b), "Performance study of FBG hoop strain sensor for pipeline leak detection and localization", *J. Aerosp. Eng.*, **31**(5), 04018050. https://doi.org/10.1061/(ASCE)AS.1943-5525.0000880.

Jia, Z.G., Ren, L., Li. H.N., Ho, S.C. and Song, G.B. (2015), "Experimental study of pipeline leak detection based on hoop strain measurement", *Struct. Control Health Monitor.*, **22**(5), 799-812. https://doi.org/10.1002/stc.1718.

Jiang, F.Y., Dong, S., Zhao, Y.L., Xie, Z.X., Guedes Soares, C. (2019), "Investigation on the deformation response of submarine pipelines subjected to impact loads by dropped objects", *Ocean Eng*., **194**, 106638. https://doi.org/10.1016/j.oceaneng.2019.106638.

Kennedy, R.P., Chow, A.M. and Williamson, R.A. (1997), "Fault movement effects on buried oil pipeline", *J. Transport. Eng.*, **103**(5), 617-633.

Kishawy, H.A. and Gabbar, H.A. (2010), "Review of pipeline integrity management practices", *J.Pressure Vessels Piping*., **87**(7), 373-380. https://doi.org/10.1016/j.ijpvp.2010.04.003.

Liu, A.H., Chen, k., Huang, X.F., Chen, J.Y., Zhou, J.F., Xu, W.B. (2019), "Corrosion failure probability analysis of buried gas pipelines based on subset simulation", *J. Loss Prevention Process Industries*, **57**, 25-33. https://doi.org/10.1016/j.jlp.2018.11.008.

Liu, B., Liu, X.J. and Zhang, H. (2009), "Strain-based design criteria of pipelines", *J. Loss Prevention Process Industries*, **22**(6), 884-888. https://doi.org/10.1016/j.jlp.2009.07.010.

Lynch, Jerome.P., Kiremidjian, A.S., Allen, D.W., Law, K.H., Carryer, Ed., Farrar, C.R., Sohn, Hoon., Nadler, B. and Wait, J.R. (2004), "Design and performance validation of a wireless sensing unit for structural monitoring applications", *Struct. Eng. Mech.*,, 17(3-4), 393-408.

Newmark, N.M. and Hall, W.J. (1975), "Pipeline design to resist large fault displacement", *The U.S National Conference on Earthquake Engineering*, 416-425.

Ren, L., Jia, Z.G., Li, H.N. and Song, G.B. (2014), "Design and experimental study on FBG hoop-strain sensor in pipeline monitoring", *Optical Fiber Technology*, **20**(1), 15-23. https://doi.org/10.1016/j.yofte.2013.11.004.

Ren, L., Jiang, T., Jia, Z.G., Li, D.S., Yuan, C.L. and Li, H.N. (2018), "Pipeline corrosion and leakage monitoring based on the distributed optical fiber sensing technology", *Measurement*, 122, 57-65. https://doi.org/10.1016/j.measurement.2018.03.018.

Rofooei, F.R., Jalali, H.H., Attari, N. K. A. and Kenarangi, H. (2015), "Samadian M. Parametric study of buried steel and high density polyethylene gas pipelines due to oblique-reverse faulting", *Canadian J. Civil Eng.*, **42**(3), 178-189. https://doi.org/10.1139/cjce-2014-0047.

Takada, S., Hassani, N. and Fukuda, K. (2001), "A new proposal for simplified design of buried steel pipes crossing active faults", *Earthq. Eng. Struct. Dynam.*, **30**(8), 1243-1257.https://doi.org/10.1002/eqe.62.

Tian, J.P., Zhang, J., Dong, F.F., Du, G.F. (2019), "Dynamic response of buried pipeline subject to impact loadsusing pie zoceramic transducers", *J. Pressure Vessels Piping*, **177**, https://doi.org/10.1016/j.ijpvp.2019.103984.

Vazouras, P., Dakoulas, P. and Karamanos, S.A. (2015), "Pipe–soil interaction and pipeline performance under strike–slip fault movements", *Soil Dynam. Earthq. Eng.*, **72**, 48-65. https://doi.org/10.1016/j.soildyn.2015.01.014.

Vazouras, P., Karamanos, S.A. and Dakoulas, P. (2012), "Mechanical behavior of buried steel pipes crossing active strike-slip faults", *Soil Dynam. Earthq. Eng.*, **41**, 164-180. https://doi.org/10.1016/j.soildyn.2012.05.012

Wang, H.K., Yu,Y., Yu, J.X., Xu,W.P., Li, X.B., Yu, S.Z. (2019), "Numerical simulation of the erosion of pipe bends considering fluid-induced stress and surface scar evolution", *Wear*, 440–441, 203043. https://doi.org/10.1016/j.wear.2019.203043.

Wang, L.R.L. and Yeh, Y.H. (1985), "A refined seismic analysis and design of buried pipeline for fault movement", *Earthq. Eng. Struct. Dynam.*, **13**(1), 75-96.

Wu, K., Zhang, H., Liu., X.B., Bolati, D., Liu, G.L. Chen, P.C., Zhao,Y.T.(2019),"Stress and strain analysis of buried PE pipeline s subjected to mechanical excavation", *Eng. Failure Anal.*, **106**, 04171.https://doi.org/10.1016/j.engfailanal.2019.104171.

Xu, L.G. and Lin, M. (2017), "Analysis of buried pipelines subjected to reverse fault motion using the vector form intrinsic finite element method", *Soil Dynam. Earthq. Eng.*, **93**, 61-83. https://doi.org/10.1016/j.soildyn.2016.12.004.

Xu, Y., Luo, M.Z., Liu,Q., Du, G.F., Song, G.B. (2019), "PZT transducer array enabled pipeline defect locating based on time-reversal method and matching pursuit de-noising", *Smart Mater. Struct.*, **28**(7), 075019. https://doi.org/10.1088/1361-665X/ab1cc9.

Yi, T.H., Zhou G.D., Li, H.N. and Zhang, X.D. (2015), "Optimal sensor placement for health monitoring of high-rise structure based on collaborative-climb monkey algorithm", *Struct. Eng. Mech.,* **54**(2), 305-317. https://doi.org/10.12989/sem.2015.54.2.305.

Zeng, L., Parvasi, S.M., Kong, Q.Z., Huo. L.S., Lim, I., Li, M. and Song, G.B. (2015), "Bond slip detection of concrete-encased composite structure using shear wave based active sensing approach", *Smart Mater. Struct.*, **24**(12), 125026. https://doi.org/10.1088/0964-1726/24/12/125026.

Zeng, X., Dong, F.F., Xie, X.D.and Du, G.F. (2019), "A new analytical method of strain and deformation of pipeline under fault movement", *J. Pressure Vessels Piping*, **172**, 199-211.https://doi.org/10.1016/j.ijpvp.2019.03.005.

Zhang, J., Xu, J.D., Guan, W.Q. and Du, G.F. (2018), "Damage Detection of Concrete-Filled Square Steel Tube (CFSST) Column Joints under Cyclic Loading Using Piezoceramic Transducers", *Sensors*, **18**(10), 3266. https://doi.org/10.3390/s18103266.

Zhang, J.C., Huang, Y.S. and Zheng, Y. (2018), "A feasibility study on timber damage detection using piezoceramic-transducer-enabled active sensing", *Sensors*, **18**(5), 1563. https://doi.org/10.3390/s18051563.

Zhang, L.S., Zhao, X.B, Yan, X.Z. and Yang, X.J. (2016), "A new finite element model of buried steel pipelines crossing strike-slip faults considering equivalent boundary springs", *Eng. Struct.*, **123**, 30-44. https://doi.org/10.1016/j.engstruct.2016.05.042.

Zhang, S.Z., Li, S.Y., Chen, S.N., Wu, Z.Z., Wang, R.J. and Duo, Y.Q. (2017), "Stress analysis on large-diameter buried gas pipelines under catastrophic landslides", *Petroleum Sci.*, **14** (3), 579-585. https://doi.org/10.1007/s12182-017-0177-y.

Zhu, J.X., Ren, L., Ho, S.C., Jia, Z.G. and Song, G.B. (2017), "Gas pipeline leakage detection based on PZT sensors", *Smart Mater. Struct.*, **26**(2), 025022. https://doi.org/10.1088/1361-665X/26/2/025022.

CC